Molecular Origin of the Selectivity Differences between Palladium and Gold–Palladium in Benzyl Alcohol Oxidation: Different Oxygen Adsorption Properties

Aditya Savara,*[a] Carine E. Chan-Thaw,[b] Jonathan E. Sutton,[a] Di Wang,[c] Laura Prati,[b] and Alberto Villa*[b]

The same mechanism and microkinetic model used for benzyl alcohol oxidation over Pd/C was shown to apply to benzyl alcohol oxidation over AuPd/C. Almost all of the selectivity differences could be explained by a decrease in oxygen adsorption on AuPd. After isolating oxygen adsorption as being the origin of the selectivity differences, density functional theory was used to investigate the oxygen adsorption properties of a pure Pd surface, a pure Au surface, and an alloyed AuPd surface. The calculations showed that Au–Pd alloying decreased the oxygen adsorption properties relative to pure Pd, which explained the selectivity differences, consistent with the microkinetic modeling.

The oxidation of benzyl alcohol by supported noble metals has been the subject of growing interest.[1] The main oxidation product is benzaldehyde, an important intermediate in the fragrances and food industry.[2] Side products, such as benzene, toluene, benzoic acid, benzyl benzoate, and benzyl ether, have also been observed.[2] Au and Pd nanoparticles are the most studied catalysts for this reaction:[1b,c,3] Pd for its resistance to deactivation and Au for its high activity.[3] Recently, attention has been devoted to Au–Pd for the liquid-phase oxidation of alcohols.[1c,4] One reason for this interest is the fact that Au and Pd can form solid solutions over the whole range of Au/Pd atomic ratios, and the addition of the second metal can alter the electronic and geometrical properties with the formation of alloy and/or core–shell structures.[5] It has been shown that alloying Au to Pd catalysts modifies the catalytic activity and selectivity.[5] For example, under specific reaction conditions, the addition of Au to Pd was shown to limit the formation of toluene, which implies a hindering of the disproportionation pathway.[3a,c,d] The chemical origin of these differences between the selectivities of AuPd and Pd in the oxidation of benzyl alcohol is not completely understood.

We previously used microkinetic modeling (simulation + fitting[6]) to validate and understand the mechanism for benzyl alcohol oxidation to various products (e.g., benzaldehyde, toluene, benzoic acid, etc.) over Pd/C.[6a] Herein, we apply the same microkinetic model based on the mechanism in Scheme 1 to understand the differences in benzyl alcohol oxidation over AuPd/C relative to that over Pd/C and then use density functional theory calculations to validate the differences in the oxygen adsorption properties inferred from the microkinetic modeling.

The temperature and concentration conditions were the same as those in our previous study (Table S1, Supporting Information),[6a] and the same microkinetic model was also used (Table S2). The AuPd/C catalyst was prepared by following a two-step procedure to produce homogenous-alloyed AuPd nanoparticles.[5b] The total metal loading was 1 wt% with a Au/Pd molar ratio of 6:4. Activated carbon X40S from Camel was used as a support. The support did not show any activity in the oxidation of benzyl alcohol under the selected reaction conditions. The high-resolution transmission electron microscopy (HRTEM) images reveal that most of the AuPd particles are multiply twinned in the form of decahedra or truncated decahedra (Figure 1).[5b] The uniform lattice spacings between the Pd (111) plane (2.25 Å) and the Au (111) plane (2.35 Å) confirm the alloy state (Figure 1).[7]

All data points here were measured at a reaction time of 60 min, which was found to be suitable for microkinetic modeling of the AuPd/C data. First, we used microkinetic modeling to reproduce the experimental data for the AuPd experiments at 70 °C. The previously obtained rate constant values for Pd/C were used as an initial guess, and this was followed by gradient optimization of the kinetic parameters (i.e., rate constants in Table 1).

Figures 2 and 3 show the results of this fitting: we see that the microkinetic model reproduces the trends for AuPd/C (red vs. black circles). The selectivity for AuPd/C differs from that of Pd/C: the experimental data points for Pd/C are shown in gray for comparison. Unlike the Pd/C data, the AuPd/C data is mostly monotonic. The simulations reproduce all of the trends over AuPd/C with mostly quantitative agreement, which indicates that the kinetic and mechanistic models are in

[a] Dr. A. Savara, Dr. J. E. Sutton
Chemical Sciences Division
Oak Ridge National Laboratory Institution
1 Bethel Valley Road MS 6201, Oak Ridge, TN 37831 (USA)
E-mail: savaraa@ornl.gov

[b] Dr. C. E. Chan-Thaw, Prof. L. Prati, Dr. A. Villa
Dipartimento di Chimica
Università degli Studi di Milano
via Golgi 19, 20133, Milano (Italy)
E-mail: alberto.villa@unimi.it

[c] Dr. D. Wang
Institute of Nanotechnology and Karlsruhe Nano Micro Facility Karlsruhe Institute of Technology
Hermann-von-Helmholtz-Platz 1,
76344 Eggenstein-Leopoldshafen (Germany)

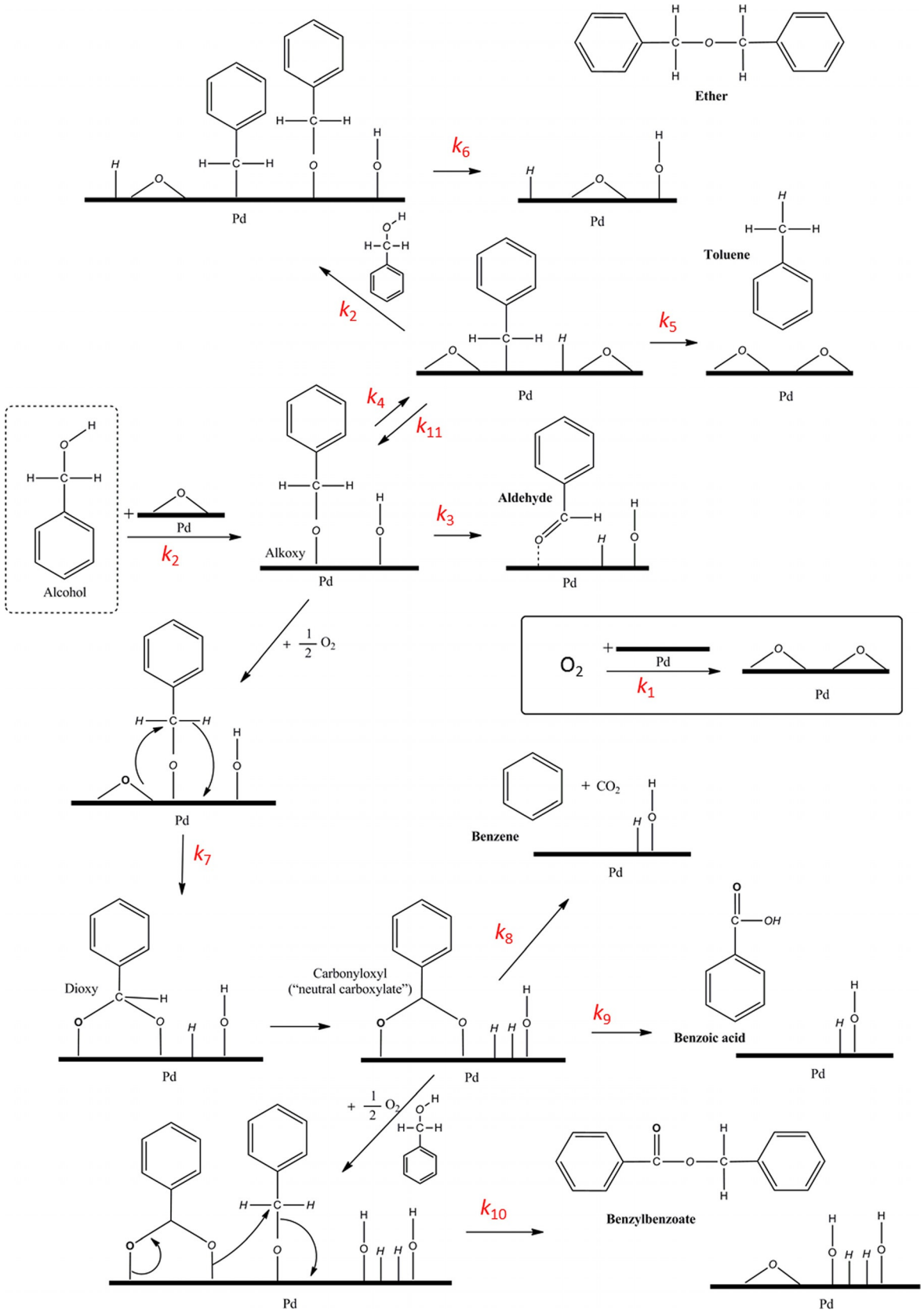

Scheme 1. Mechanism with sufficient detail for microkinetic modeling. This scheme is reproduced from Ref. [6a] with permission from Wiley VCH.

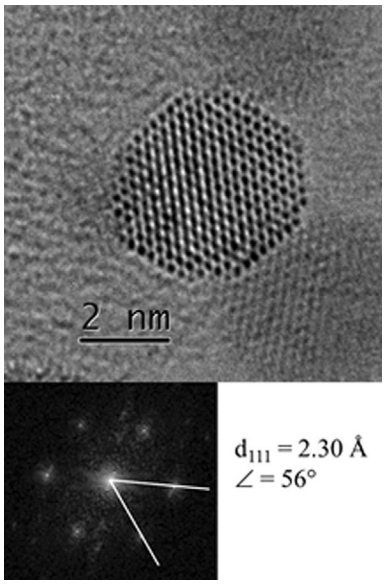

Figure 1. Representative HRTEM image of a multiply twinned particle in the form of truncated decahedron configuration with insets showing the fast Fourier transformations.

Table 1. Fitted rate constants from the microkinetic model at 70 °C.[a]

Rate constant	Value for Pd/C[b]	Value for AuPd/C (this study)
k_1	8.2×10^{0} s^{-1}bar^{-1}	1.6×10^{0} s^{-1}bar^{-1}
k_2	1.4×10^{-1} s^{-1}mol^{-1}L	1.6×10^{-1} s^{-1}bar^{-1}
k_3	5.1×10^{6} s^{-1}	4.2×10^{6} s^{-1}
k_4	6.7×10^{8} s^{-1}	6.2×10^{8} s^{-1}
k_5	4.4×10^{14} s^{-1}	1.6×10^{14} s^{-1}
k_6	2.9×10^{11} s^{-1}	6.1×10^{11} s^{-1}
k_7	1.6×10^{6} s^{-1}	1.4×10^{6} s^{-1}
k_8	1.4×10^{14} s^{-1}	1.6×10^{14} s^{-1}
k_9	5.5×10^{14} s^{-1}	5.5×10^{14} s^{-1}
k_{10}	9.4×10^{12} s^{-1}	5.4×10^{12} s^{-1}
k_{11}	2.2×10^{11} s^{-1}	2.2×10^{11} s^{-1}

[a] For AuPd, the amount of benzene produced at 70 °C was too low to detect. The value provided for k_8 at 70 °C was determined by gradient optimization during fitting of the temperature dependent data. [b] Data were taken from Ref. [6]

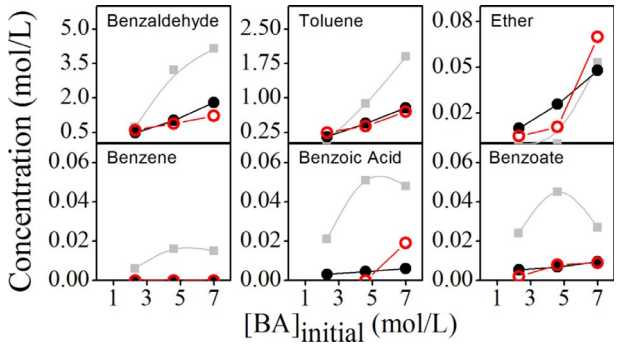

Figure 2. Trends for AuPd/C expressed as concentration of products versus initial concentration of benzyl alcohol (BA). Experimental points: ○, microkinetic model: ●. Experimental data points from Pd/C are shown in gray for comparison.

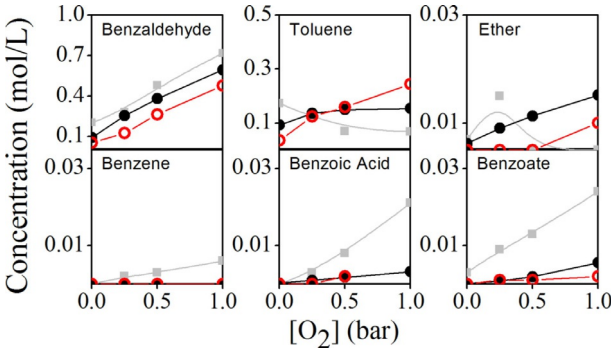

Figure 3. Trends for AuPd/C expressed as the concentration of products versus oxygen pressure. Experimental data points from Pd/C are shown in gray for comparison.

accordance with the experiments. The rate constants obtained from fitting are shown in Table 1, alongside the rate constants previously obtained for Pd/C. Under these conditions, AuPd/C has lower activity than Pd/C and shows a different product distribution with less formation of products from the "carbonyloxyl" pathway (e.g., benzene, benzoic acid, benzoate) (Table 2).[3d] Different selectivity is obtained over Pd/TiO_2 and AuPd/TiO_2 [60 °C, pO_2 = 2 bar (1 bar = 0.1 MPa), toluene as solvent].[8] It is clear that the support and the reaction conditions can affect the selectivity and mechanism of alcohol oxidation over Pd versus AuPd. In this study, the carbon support is inactive for the reaction and enables us to compare the selectivity over the different particles directly.

Table 2. Comparison of the activity and selectivities of Pd/C and AuPd/C.[a]

Catalyst[b]	Selectivity [%]					
	Aldehyde	Toluene	Benzene	Acid	Ether	Benzoate
Pd/C	83	7.9	0.70	2.4	0	5.5
AuPd/C	65	33	0	0	1.3	0.54

[a] 25% Benzyl alcohol/75% xylene (*v*/*v*), 70 °C, 1 bar O_2 (flow 30 mL min^{-1}). [b] C = activated carbon.

As shown in Figure 4, the differences between palladium and AuPd are almost entirely due to k_1: Figure 4 shows the ratios of the logs of the rate constants for AuPd/C versus Pd/C, for which the largest change (by far) on this log scale is in k_1. Nearly all of the selectivity changes can be explained by this change in k_1, which corresponds to oxygen adsorption. This finding makes sense in the context of our mechanistic studies: the aldehyde route and the carbonyloxyl pathways both require surface oxygen, whereas the toluene route is facilitated by a lack of surface oxygen. Figure 5 shows this selectivity difference and also shows that increasing the oxygen pressure has less of an effect over AuPd than over Pd. To strengthen this point and to validate the idea that oxygen adsorption would be different on the AuPd surface versus the Pd surface,

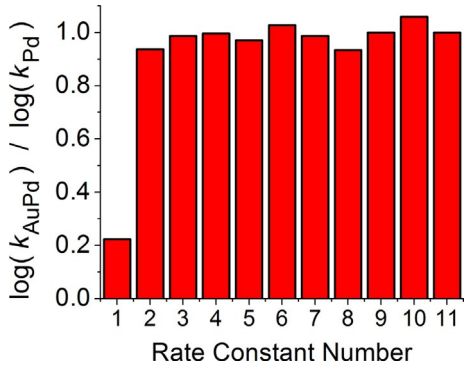

Figure 4. Ratios of the logs of the rate constants between AuPd/C and Pd/C, for which the largest change on this scale is in k_1.

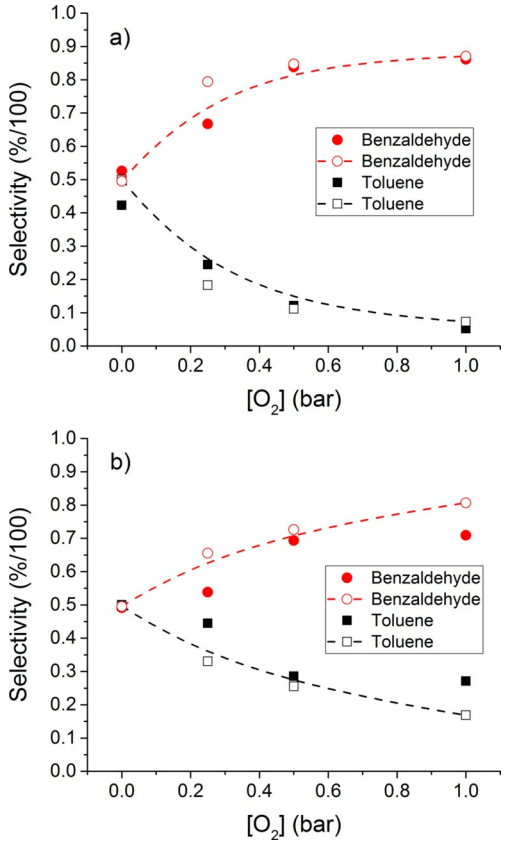

Figure 5. Oxygen dependence of the selectivities towards toluene and alde hyde over for the same reaction conditions as those described in Table 2. Panel a is for Pd and panel b is for AuPd. Solid symbols are from experiment, whereas open symbols are from microkinetic modeling simulations. The dashed lines are guides for the eye.

DFT calculations on the strength and activation energies of oxygen adsorption on Pd and AuPd were performed (Table 3).

The binding strength and activation energies for O_2 adsorption to the most stable initial and final states over the most stable alloy were calculated after calculating the energies of 100 different random configurations of AuPd alloys as well as a number of nonrandom ordered structures. The lowest energy AuPd alloy in our dataset is a nonordered (no symmetry) configuration that is shown in Figure 6 (more details are provided in the Supporting Information). The results of these calculations are provided in Table 3. Energy profiles and images of the dissociation pathways are depicted in Figures 6 and S2. We see that the oxygen energetics display the expected behavior: the energy of adsorption on the AuPd alloy has a value between those on Au and Pd, such that the total amount of oxygen binding and activation are both reduced relative to those on pure Pd, consistent with our experimental results.

As in our previous microkinetic study, we used the initial rate of change in aldehyde production to obtain an apparent activation energy: here we obtained a value of 44.5 kJ mol^{-1} (Figure 7), which reflects the activation energy of alcohol absorption, E_{a2}, as shown by the previous study and consistent with the literature.

Table 3. Results of DFT calculations for the energies of adsorption and activation of O_2 on pure Pd and Au and the most stable of the AuPd alloys checked.[a]

Surface	$O_{2(ads)}$ Binding energy [kJ mol^{-1}]	$2\,O_{(ads)}$ Binding energy [kJ mol^{-1}]	Activation energy [kJ mol^{-1}]
Pd	90	247	55
Au	6	33	98
AuPd	5	53	92

[a] Binding energies are with respect to clean slabs and gas phase O_2. A positive binding energy denotes a repulsive interaction between the mol ecule and the surface.

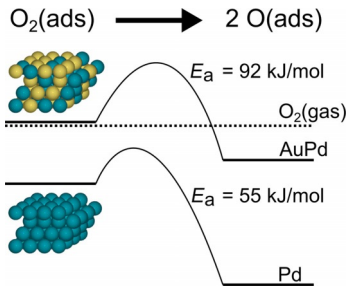

Figure 6. Energy profiles for O_2 dissociation on the AuPd alloy surface and the pure Pd alloy surface, with the gas phase O_2 chemical potential shown for reference.

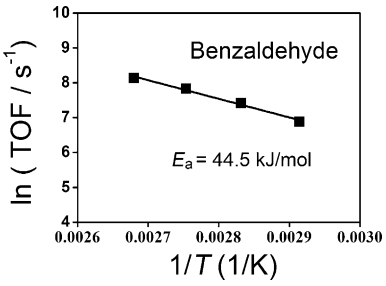

Figure 7. Arrhenius type plot with the natural log of the early time turnover frequency (TOF) versus 1/*T* for benzaldehyde formation. Apparent activation energies were extracted from the slopes.

Plugging in this value of 44.5 kJ mol^{-1} for E_{a2} into the microkinetic model, we are able to reproduce most of the temperature dependence observed experimentally but not the 90–100 °C benzoic acid production and benzene production. The activation energies for the reactions associated with benzoic acid production and benzene production (E_{a8} and E_{a9}) were raised until a good fit was found, with E_{a8} = 285 kJ mol^{-1} and E_{a9} = 143 kJ mol^{-1}. This set of parameters reproduces the trends observed experimentally for all six products, with mostly quantitative agreement (Figure 8).

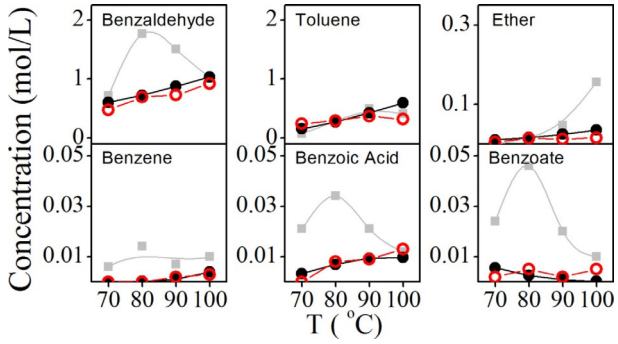

Figure 8. Trends in the temperature dependence of the products obtained in the oxidation of benzyl alcohol over AuPd/C. Experimental points: ○, microkinetic model: ●. Experimental data points from Pd/C are shown in gray for comparison.

As noted earlier, we find that the same microkinetic model used for Pd/C in the previous study[6] is able to reproduce all of the trends for AuPd/C correctly and captures the differences between AuPd/C and Pd/C. For AuPd/C, we find that the temperature dependence is mostly governed by the activation energy of k_2 (alcohol adsorption), which is also found in the microkinetic modeling of the reaction over Pd/C and is consistent with past literature.[6]

In summary, the same microkinetic model used for Pd/C was able to produce the AuPd/C data. It was expected that AuPd/C would bind oxygen less strongly than Pd/C. Remarkably, almost all of the selectivity changes observed between Pd/C and AuPd/C could be explained by a decrease in oxygen adsorption (as a result of a decrease in k_1). No excited state electron transfer or any special local configuration of Au and Pd atoms was required to reproduce the experimental data produced by using AuPd.

Acknowledgements

The kinetic simulations and DFT calculations were supported by the U.S. Department of Energy, Office of Science, Basic Energy Sciences, Chemical Sciences, Geosciences, and Biosciences Division. This research used resources of the Oak Ridge Leadership Computing Facility at the Oak Ridge National Laboratory, which is supported by the Office of Science of the U.S. Department of Energy under Contract No. DE-AC05-00OR22725. TEM work was supported by Karlsruhe Nano Micro Facility (KNMF) long term project.

Keywords: alloys · density functional calculations · gold · oxidation · palladium

[1] a) M. Besson, P. Gallezot, *Catal. Today* **2000**, *57*, 127 141; b) T. Mallat, A. Baiker, *Chem. Rev.* **2004**, *104*, 3037 3058; c) N. Dimitratos, J. A. Lopez Sanchez, G. J. Hutchings, *Chem. Sci.* **2012**, *3*, 20 44; d) S. E. Davis, M. S. Ide, R. J. Davis, *Green Chem.* **2013**, *15*, 17 45.

[2] a) J. Luo, H. Yu, H. J. Wang, H. H. Wang, F. Peng, *Chem. Eng. J.* **2014**, *240*, 434 442; b) Y. Yu, B. Lu, X. Wang, J. Zhao, X. Wang, Q. Cai, *Chem. Eng. J.* **2010**, *162*, 738 742.

[3] a) C. Keresszegi, D. Ferri, T. Mallat, A. Baiker, *J. Catal.* **2005**, *234*, 64 75; b) D. Ferri, C. Mondelli, F. Krumeich, A. Baiker, *J Phys Chem. B* **2006**, *110*, 22982 22986A; c) S. Meenakshisundaram, E. Nowicka, P. J. Miedziak, G. L. Brett, R. L. Jenkins, N. Dimitratos, S. H. Taylor, D. W. Knight, D. Bethell, G. J. Hutchings, *Faraday Discuss.* **2010**, *145*, 341 356; d) A. Savara, C. E. Chan Thaw, I. Rossetti, A. Villa, L. Prati, *ChemCatChem* **2014**, *6*, 3464 3473; e) C. Keresszegi, D. Ferri, T. Mallat, A. Baiker, *J. Phys. Chem. B* **2005**, *109*, 958 967; f) A. Villa, N. Dimitratos, C. E. Chan Thaw, C. Hammond, G. M. Veith, D. Wang, M. Manzoli, L. Prati G. J. Hutchings, *Chem. Soc. Rev.* **2016**, *45*, 4953 4994.

[4] a) F. Gao, D. W. Goodmani, *Chem. Soc. Rev.* **2012**, *41*, 8009 8020; b) A. Villa, D. Wang, D. Su, L. Prati, *Catal. Sci. Technol.* **2015**, *5*, 55 68; c) G. Collins, J. D. Holmes, *Adv. Mater.* **2016**, *28*, 5689 5695.

[5] a) M. Chen, D. Kumar, C. W. Yi, D. W. Goodman, *Science* **2005**, *310*, 291 293; b) D. Wang, A. Villa, F. Porta, D. Su, L. Prati, *Chem. Commun.* **2006**, 1956 1958; c) D. I. Enache, J. K. Edwards, P. Landon, B. Solsona Espriu, A. F. Carley, A. A. Herzing, M. Watanabe, C. J. Kiely, D. W. Knight, G. J. Hutchings, *Science* **2006**, *311*, 362 365; d) W. Hou, N. A. Dehm, R. W. J. Scott, *J. Catal.* **2008**, *253*, 22 27; e) A. Villa, D. Wang, N. Dimitratos, D. Su, V. Trevisan, L. Prati, *Catal. Today* **2010**, *150*, 8 15; f) A. Villa, D. Wang, D. Su, G. Veith, L. Prati, *Phys. Chem. Chem. Phys.* **2010**, *12*, 2183 2189.

[6] a) A. Savara, I. Rossetti, C. E. Chan Thaw, L. Prati, A. Villa, *ChemCatChem* **2016**, *8*, 2482 2491; b) A. Savara, *Surf. Sci.* **2016**, *653*, 169 180.

[7] a) A. R. Denton, N. W. Ashcroft, *Phys. Rev. A* **1991**, *43*, 3161 3164; b) S. C. Y. Tsen, P. A. Crozier, J. Liu, *Ultramicroscopy* **2003**, *98*, 63 72.

[8] A. Villa, D. Ferri, S. Campisi, C. E. Chan Thaw, Y. Lu, O. Kröcher, L. Prati, *ChemCatChem* **2015**, *7*, 2534 2541.